Annals of Botany **113**: 617–627, 2014
doi:10.1093/aob/mct294, available online at www.aob.oxfordjournals.org

ANNALS OF BOTANY
Founded 1887

Contrasting hydraulic architecture and function in deep and shallow roots of tree species from a semi-arid habitat

Daniel M. Johnson[1,*], Craig R. Brodersen[2], Mary Reed[2], Jean-Christophe Domec[1,3] and Robert B. Jackson[1]

[1]*Nicholas School of the Environment, Duke University, Durham, NC 27708, USA,* [2]*Citrus Research and Education Center, University of Florida, Lake Alfred, FL 33850, USA and* [3]*University of Bordeaux, Bordeaux Sciences AGRO, UMR 1220 TCEM INRA, 1 Cours du général de Gaulle, 33175 Gradignan Cedex, France*
** For correspondence. E-mail dan.johnson@duke.edu*

Received: 20 July 2013 Returned for revision: 14 October 2013 Accepted: 18 November 2013 Published electronically: 20 December 2013

• *Background and Aims* Despite the importance of vessels in angiosperm roots for plant water transport, there is little research on the microanatomy of woody plant roots. Vessels in roots can be interconnected networks or nearly solitary, with few vessel–vessel connections. Species with few connections are common in arid habitats, presumably to isolate embolisms. In this study, measurements were made of root vessel pit sizes, vessel air-seeding pressures, pit membrane thicknesses and the degree of vessel interconnectedness in deep (approx. 20 m) and shallow (<10 cm) roots of two co-occurring species, *Sideroxylon lanuginosum* and *Quercus fusiformis*.
• *Methods* Scanning electron microscopy was used to image pit dimensions and to measure the distance between connected vessels. The number of connected vessels in larger samples was determined by using high-resolution computed tomography and three-dimensional (3-D) image analysis. Individual vessel air-seeding pressures were measured using a microcapillary method. The thickness of pit membranes was measured using transmission electron microscopy.
• *Key Results* Vessel pit size varied across both species and rooting depths. Deep *Q. fusiformis* roots had the largest pits overall (>500 μm) and more large pits than either shallow *Q. fusiformis* roots or *S. lanuginosum* roots. Vessel air-seeding pressures were approximately four times greater in *Q. fusiformis* than in *S. lanuginosum* and 1·3–1·9 times greater in shallow roots than in deep roots. *Sideroxylon lanuginosum* had 34–44 % of its vessels interconnected, whereas *Q. fusiformis* only had 1–6 % of its vessels connected. Vessel air-seeding pressures were unrelated to pit membrane thickness but showed a positive relationship with vessel interconnectedness.
• *Conclusions* These data support the hypothesis that species with more vessel–vessel integration are often less resistant to embolism than species with isolated vessels. This study also highlights the usefulness of tomography for vessel network analysis and the important role of 3-D xylem organization in plant hydraulic function.

Key words: Anatomy, cavitation, drought, embolism, high-resolution computed tomography, *Quercus fusiformis*, root integration, *Sideroxylon lanuginosum*, water potential, xylem vessels, X-ray.

INTRODUCTION

Root water uptake and hydraulic transport through xylem are critical for plant functioning and survival. Since the primary pathway for water flow into plants is through the root system, disruption of this flow could result in strong negative effects on plant water status. While many studies have examined water transport characteristics from the base to the top of a tree (e.g. Tyree and Ewers, 1991; Cruiziat *et al.*, 2002; Tyree and Zimmermann, 2002), half or more of the hydraulic pathway remains unstudied in many species and ecosystems (Canadell *et al.*, 1996; Schenk and Jackson, 2002, 2005; Oliveira *et al.*, 2005; Pratt *et al.*, 2007; West *et al.*, 2007).

Although the root hydraulic pathway is of great functional importance, root hydraulics are far less studied and understood than shoot hydraulics, largely due to their relative inaccessibility and fragile nature, especially in smaller roots. Regulation of water flow across roots is well described by a composite transport model that identifies hydraulic resistances across tissue types, including the suberized endodermis (Steudle and Petersen, 1998). In its path to the xylem, water encounters radial resistance from several layers of living cells. On the radial and axial root axis, these resistances depend on root anatomy (Steudle and Peterson, 1998), whereas protein water channels (aquaporins) that regulate the resistance of the transcellular pathway also play a role (Luu and Maurel, 2005; McElrone *et al.*, 2007; Maurel *et al.*, 2008). Although the largest resistance to water flow in well-hydrated roots is the radial flow from root tip to xylem (see Tyree, 2003, and references therein), embolism in xylem elements can result in large decreases in root hydraulic conductance during drought (e.g. Domec *et al.*, 2006).

Xylem structure helps determine the hydraulic conductance, embolism resistance and degree of embolism spread in roots and stems (Sperry and Pockman, 1993; Zwieniecki and Holbrook, 1998; Jackson *et al.*, 2000; Jacobsen *et al.*, 2007). Hydraulic modularity is seen as an adaptation for isolating embolized xylem conduits or sectors during drought, thus preventing the entire plant from xylem dysfunction and, potentially, death. Woody species in dry environments have been shown to have reduced hydraulic integration (i.e. fewer lateral vessel–vessel connections) and increased modularity compared with those in mesic environments (Waisel *et al.*, 1974; Schenk *et al.*, 2008).

Additionally, hydraulic modularity is much more common in species with ring-porous than those with diffuse-porous wood (Zimmerman and Brown, 1971). In the most extreme case of hydraulic modularity, one root vessel can be connected to a single branch alone (David *et al.* 2012). However, hydraulic modularity and ring porosity, with its associated large diameter vessels, are thought to be particularly adaptive in seasonally dry habitats (Orians *et al.*, 2005, and references therein). Early in the growing season when water is plentiful, large diameter vessels are produced and allow for high volume water transport. The trade-off, however, is that large diameter vessels are often more vulnerable to cavitation (Hargrave *et al.*, 1994; Choat *et al.*, 2003). As the growing season progresses and water becomes scarcer, vessels are produced that have smaller diameters. This reduction in diameter coincides with lower transport requirements and the increasing probability of embolism formation as xylem tensions increase. This seasonal and spatial modularity prevents xylem embolisms from spreading during times of water scarcity.

The Edwards Plateau region of central Texas represents an ideal system in which to study deep and shallow root hydraulic anatomy and function because of its seasonally dry climate and its system of caves, which provide access to deep roots. The region has a sub-tropical, sub-humid climate with hot summers and dry winters. Precipitation in this seasonally dry region ranges from 400 to 800 mm, and its karst topography allows us to examine root functioning *in situ* in the numerous caves found there (Jackson *et al.*, 1999; McElrone *et al.*, 2004, 2007; Bleby *et al.*, 2010). Our objectives in this study were to compare the anatomy of deep (approx. 20 m) and shallow (<10 cm) roots, including the degree of hydraulic integration and resistance to vessel embolism, in two co-occurring species with ring-porous wood: one hydraulically integrated species (*Sideroxylon lanuginosum*) and one hydraulically modular species (*Quercus fusiformis*). The root systems of species within this region at shallow and deep soil depths have been previously described (Jackson *et al.*, 1999; McElrone *et al.*, 2004). Moving vertically from root to leaf, xylem tensions are known to increase (e.g. Wiebe and Brown, 1970) and the root systems are typically the most vulnerable segment of the woody portion of the pathway (McElrone *et al.*, 2004; Choat *et al.*, 2005, Johnson *et al.*, 2013). Access to the deep cave roots of these species at approx. 20 m depth offers a unique opportunity to expand our understanding of the hydraulic organization of the xylem network below ground. Our measurements were designed to assess the hydraulic architecture and safety of the xylem networks at different points along the root hydraulic pathway. Specifically, we hypothesized that, due to the lack of water stress at 20 m depth, deep root vessels should be more vulnerable to embolism and more highly connected than shallow root vessels. Additionally, we hypothesized that pit membrane thickness should be correlated with vessel embolism resistance.

METHODS

Access to roots/root collection

At Powell's cave in Menard County, central Texas (see Jackson *et al.*, 1999; McElrone *et al.*, 2004, 2007; Bleby *et al.*, 2010), deep roots of *Sideroxylon lanuginosum* Michx. (Sapotaceae; formerly *Bumelia lanuginosa*) and *Quercus fusiformis* Small (Fagaceae) were accessed via an approx. 20 m deep cave system, and shallow roots (<10 cm) of the same species were excavated from shallow soils and traced back to their parent trees. Samples were shipped back to the lab for storage at either −20 °C or room temperature in a 50:50 distilled water:-ethanol solution, depending on the analysis.

Roots were imaged using different types of microscopy, and the vulnerability of root vessels to embolism was measured. We used scanning electron microscopy (SEM) to analyse pit sizes and distributions. High-resolution computed tomography (HRCT) was used to analyse vessel connections, the three-dimensional (3-D) xylem network and overall vessel size distributions. We used transmission electron microscopy (TEM) to analyse pit membrane thickness, as pit membrane thickness is probably responsible for differences in vessel vulnerability to embolism.

SEM sample preparation

Two samples were taken per root for SEM analysis, with 18–26 individual samples for each species and depth used for SEM imaging (for a total of 9–13 roots per species and depth). Shallow roots were collected from different individual trees (9–13 individual trees per species) and deep roots were collected in two different areas (approx. 500 m apart) of Powell's cave. As we did not identify deep roots to individual trees, we assume conservatively that we only sampled two trees (one from each location) although it is likely that we were sampling many more based on the fact that these trees grow in groves consisting of many individuals.

Samples of root tissue were hand-sectioned longitudinally into various thicknesses (approx. 0·5 to 2 mm). The sections were placed into glass dishes containing a 50:50 water:ethanol solution and were left to equilibrate for about 2 h. Sections were then exposed to a series of dehydration solutions and left to equilibrate for approximately an additional 2 h in each solution before being placed in the next solution. The order of the dehydration solutions was 50:50 distilled water:ethanol, 25:75 distilled water:ethanol, 10:90 distilled water:ethanol, 100 % ethanol, 50:50 ethanol:HMDS (hexamethydisilizane, Sigma-Aldrich, St Louis, MO, USA) and 100 % HMDS. After equilibrating in the last solution, samples were removed from the solution and allowed to air-dry overnight. Samples were then mounted onto aluminium stubs using double-sided carbon tape (Electron Microscopy Sciences, Hatfield, PA, USA).

SEM imaging

Samples were placed onto the stage of a FEI XL30 environmental scanning electron microscope (FEI, Hillsboro, OR, USA) and were imaged in variable pressure mode. An accelerating voltage of 20 kV was used for imaging. For all images used for quantitative analysis (e.g. pit membrane area per pit area), the image was centred and focused using the lowest magnification (approx. ×50). The magnification was then increased to approx. ×2000–5000 depending on the sample, allowing us to 'sample' at random, because the structures visible at high magnification could not be seen at lower magnification. The degree of magnification (×2000–5000) depended on whether we wanted

information on pit distributions across a relatively large vessel wall area (e.g. approx. 10 000 μm^2) or a smaller area (e.g. a field containing 5–10 pits, approx. 1000 μm^2). Estimates of individual pit areas and pit area per vessel area were obtained using ImageJ image analysis software (National Institutes of Health, USA; http://rsb.info.nih.gov/ij/). SEM image analysis was also used to establish a minimum threshold distance value that could be used to determine whether vessels were connected (determined at low magnification), because the HCRT image (see below) could not consistently resolve the scalariform pitting characteristic of intervessel pitting. Additionally, to assess the possibility of shrinkage in the SEM samples, the distance between adjacent vessels was checked using light microscopy on fresh samples and did not differ from the distances measured by SEM. We measured 768–1027 individual pits per species and depth for pit aperture area, and 19–26 images per species and depth for pit area to vessel area ratios. Pit area per vessel area ratios were analysed using a two-way analysis of variance (ANOVA), followed by post-hoc Bonferroni tests to test for differences between depths and species. Pit shapes were classified according to Carlquist (2001) and Wheeler (2011).

HRCT imaging

Root samples were collected from two different individual trees per species and depth at the cave site, wrapped in a moist paper towel, sealed in a plastic bag and sent overnight to the Lawrence Berkeley National Laboratory Advanced Light Source, Beamline 8·3.2 microtomography facility. Straight sections of root tissue approx. 6 cm long were excised with a razor blade from the root samples and wrapped in Parafilm to prevent dehydration during scanning. The samples were then mounted in the microtomography instrument and imaged at 15 keV in 0·25 ° increments over 180 ° following the methods of Brodersen *et al.* (2011). The 720 resulting 2-D projection images were first normalized using a custom filter in FIJI image processing software (www.fiji.sc, a Java-based distribution of ImageJ) and then reconstructed into a 3-D data set representing 3·5 mm in root length using Octopus 8·0 software (Institute for Nuclear Sciences, University of Ghent, Belgium). A second scan of equal length was performed immediately below the first scan. The two data sets were merged together in the *z*-axis using Avizo 7·0.1 software (VSG Inc., Burlington, MA, USA) to form a single, continuous 7 mm long data set with a voxel (volumetric pixel element) size of 4·5 μm^3 for the *x*, *y* and *z* co-ordinates. This process yielded a total of approx. 1500 serial sections through each individual root sample. The entire process was repeated twice (i.e. two root samples) for each species and depth, resulting in eight 3-D data sets.

Xylem connectivity

To determine the degree of connectivity between xylem vessels in each species at each depth, the distance between neighbouring vessels was analysed in 3-D using the HRCT images (see Supplementary Data Fig. S1). First, each 3-D data set was visualized with Avizo 7·0.1 software to identify vessels in close proximity, specifically where vessel walls were <30 μm apart in a single transverse plane. We used 54–68 SEM images of vessel–vessel pairs per species and depth to determine the maximum double wall thickness between vessel pairs. This analysis revealed that the maximum intervessel distance between connected *S. lanuginosum* vessels was 19·7 and 18·73 μm in deep and shallow roots, respectively (see 'SEM imaging' methods). These distances were then used as threshold criteria for distinguishing between connected and unconnected vessels in the HRCT images. One transverse slice was selected from the data set, and the distance between neighbouring vessel pairs was calculated using the 3-D measurement tool in Avizo. If the distance between the walls of each vessel pair was less than or equal to the threshold distance, then the *x*, *y* and *z* co-ordinates of the connection were recorded and given a unique identification number. Then, using the 3-D visualization capabilities of Avizo, the connections were studied axially above and below the slice used for connectivity measurements to determine whether the connections were continuous throughout the sample. Because connections between *Q. fusiformis* vessels were rare, the entire data set was utilized to search for putative connections. If any vessels appeared to be connected, a slice in the *yz* axis was applied to determine the connection following the methods used for *S. lanuginosum*. The data were then exported and analysed in Excel and SigmaPlot 11·0 (Systat Software Inc., Chicago, IL, USA) for vessel connectivity and vessel diameters. A two-way ANOVA with post-hoc Bonferroni tests was used to test for differences in vessel–vessel distances between depths and species.

TEM methods

For TEM analysis, four deep *S. lanuginosum* roots, four deep *Q. fusiformis* roots, three shallow *S. lanuginosum* roots and two shallow *Q. fusiformis* roots were used for measuring pit membrane thickness. The shallow roots were collected from different individual trees and the deep roots came from the two separate collection areas in the cave (see SEM sample preparation, above). Only two root samples of shallow *Q. fusiformis* were used due to the difficulty in finding vessel–vessel connections in these samples.

Samples were cut and fixed overnight in 3 % glutaraldehyde at 4 °C. After washing the samples three times in a potassium phosphate buffer, they were fixed again in a 2 % buffered solution of osmium tetroxide for 4 h under refrigeration. The samples were washed with buffer and dehydrated through a series of acetone concentrations (10, 20, 30,…, 80, 90, 100 %). Once the samples were infiltrated with resin by gradually replacing the acetone with Spurr's resin over several days, they were embedded and polymerized in an oven at 70 °C for 2 d. The blocks were trimmed down using a single-edge razor blade and sectioned using a Reichert-Jung Ultracut E (Vienna, Austria) ultramicrotome. Twelve 1 μm transverse sections were taken from each block using glass knives, heat-fixed to slides, stained with methylene blue–azure A and basic fuchsin, and mounted with immersion oil. Using the slide as a reference, the blocks were narrowed down to an area no larger than 1 mm^2 with a double-edge razor blade. Ultrathin (between 60 and 95 nm) sections were taken and placed onto Formvar-coated 200 mesh copper grids (Ted Pella, Inc., Redding, CA, USA). Each grid was stained in a 2 % uranyl acetate solution for 15 min, washed thoroughly with filtered deionized water, then stained with lead citrate for 5 min and washed in alternating

streams of filtered deionized water and filtered 0·02 N sodium hydroxide twice each. Images were then taken of intervessel pit membranes using a FEI Morgagni 268 transmission electron microscope at 80kV accelerating voltage. Six different pit membranes were imaged for each sample. Image analysis was executed using FIJI software, with ten measurements taken along each pit membrane. Pit membrane thickness was analysed using a paired two-sample *t*-test to determine an average membrane width, and statistical differences between depths and species were determined with post-hoc Bonferroni analysis in SigmaPlot.

Air-seeding threshold

To determine the pressure required to push air across the pit membranes of individual vessels, the microcapillary technique of Choat *et al.* (2006) was utilized. The positive pressure applied to the vessel lumen is equal to but opposite in sign to the tension necessary to pull air from a neighbouring air-filled vessel into a functional vessel. Fresh root samples from the cave site were sent overnight to the lab and stored at 4 °C until the measurements were performed (<24 h). Six roots per species and depth were used for the air-seeding measurements and one vessel per root was measured. Each of the shallow roots was from a different tree, but deep roots came from two different collection sites in the cave (see SEM preparation methods, above). Root segments approx. 6 cm in length were cut underwater from the larger samples. Segments were then secured in a multipoint articulating vice (Panavise #209, Panavise Inc., Reno, NV, USA) and the cut transverse surface was viewed under a dissecting microscope. A digital photograph was then taken of the transverse surface, a vessel was selected for capillary tube insertion and the vessel diameter was measured using FIJI software. Next, a glass microcapillary tube (Model #1B100-4, 0·58 mm inner diameter, World Precision Instruments, Sarasota, FL, USA) pulled to a tip diameter of approx. 15 μm (using a Stoelting Vertical Pipette Puller, Stoelting Co., Wood Dale, IL, USA) was inserted by hand into a single vessel. The microcapillary tube was then sealed in place using a cyanoacrylic glue (Loctite #409, Henkel Corp., Rocky Hill, CT, USA) and hardening accelerant (Loctite #7452). The microcapillary tube was mounted in a modified capillary tube holder (Stoelting Co., Model #51442) attached to a 1 m length of PEEK tubing (0·76 mm inner diameter, Victrex USA Inc., West Conshohocken, PA, USA) with its terminus located in a Scholander style pressure chamber (Model #1505 D, PMS Instrument Company, Albany, OR, USA). The capillary holder was mounted on a ring stand such that the distal end of the segment was below the surface of water in a 500 mL beaker. Low pressure was then applied to the vessel (<0·05 MPa). If air bubbles were visibly exiting the distal end of the stem, it was determined that the vessel spanned the entire length of the segment and the segment was discarded. For every one sample that did not have the vessel open at the distal end, there were approx. 4–5 samples that did. Next, the pressure was increased at a rate of 0·5 MPa min^{-1} until air bubbles were observed exiting the distal end of the segment. The positive pressure at this point was recorded as the air-seeding pressure. A two-way ANOVA was performed to test for differences in air-seeding pressure in each species and depth (deep vs. shallow) and a sigmoidal regression was used to determine the relationship between air-seeding pressure and the fraction of connected vessels.

Theoretical hydraulic conductivity and predicted pore diameters

Theoretical hydraulic conductivity (K_s) was calculated by using the Hagen–Poiseuille equation:

$$K_s = \left(\pi\rho/128\eta A\right) \times \Sigma d^4$$

where ρ is the density of water at 20 °C (998·2 kg m^{-3}), η is the viscosity of water at 20 °C (1·002 × 10^{-9} MPa s), A is the cross-sectional root area and d is the individual vessel diameter. Individual vessel diameter distributions are presented in Supplementary Data Fig. S1. These data were compared with published measured values of hydraulic conductivity (McElrone *et al.*, 2004), and the percentage differences between theoretical and measured conductivity were determined.

Following the methods of Jansen *et al.* (2009), we calculated the theoretical pore diameters inside the pit membranes based on our measured air-seeding threshold values. Theoretical pore diameter (D_T) was calculated as:

$$D_T = 4\Upsilon\cos\Theta/P_a,$$

where Υ is the surface tension of water, Θ is the contact angle (assumed to be 0), and P_a is the measured air-seeding threshold.

RESULTS

Morphological characteristics of root xylem networks

We observed a great deal of variation in the size and structure of the xylem network components in the two species across the two depths where the root samples were collected. When viewed in transverse cross-section, *Q. fusiformis* roots had significantly larger vessel diameters as compared with *S. lanuginosum*. Deep *Q. fusiformis* root vessels were distributed evenly through the xylem area, whereas roots in shallow vessels were divided into discrete sectors (Figs 1, 2) with thick bands of parenchyma tissue delineating the vessel groups. There were no obvious sectoring patterns in *S. lanuginosum* xylem at either depth. The mean distance between adjacent vessels for shallow *Q. fusiformis* roots was 160 μm, which was greater than the vessel–vessel distance in deep *Q. fusiformis* roots, deep *S. lanuginosum* roots or shallow *S. lanuginosum* roots (mean vessel–vessel distance ranged from 60 to 82 μm in deep *Q. fusiformis*, shallow *S. lanuginosum* and deep *S. lanuginosum* roots, $P < 0.0001$, Fig. 3A). Network analysis using HRCT imaging revealed more vessel–vessel connections in *S. lanuginosum* than in *Q. fusiformis* (Table 1, Figs 1, 2). Between 34 and 44 % of vessels had connections to other vessels in *S. lanuginosum*, but only 1–6 % had connections in *Q. fusiformis*.

Variability in vessel wall ultrastructure

An SEM and TEM analysis of vessel wall ultrastructure revealed further details about the connectivity of the xylem networks. Vessel walls imaged with SEM showed that deep and shallow roots of both species had a large variation in the size

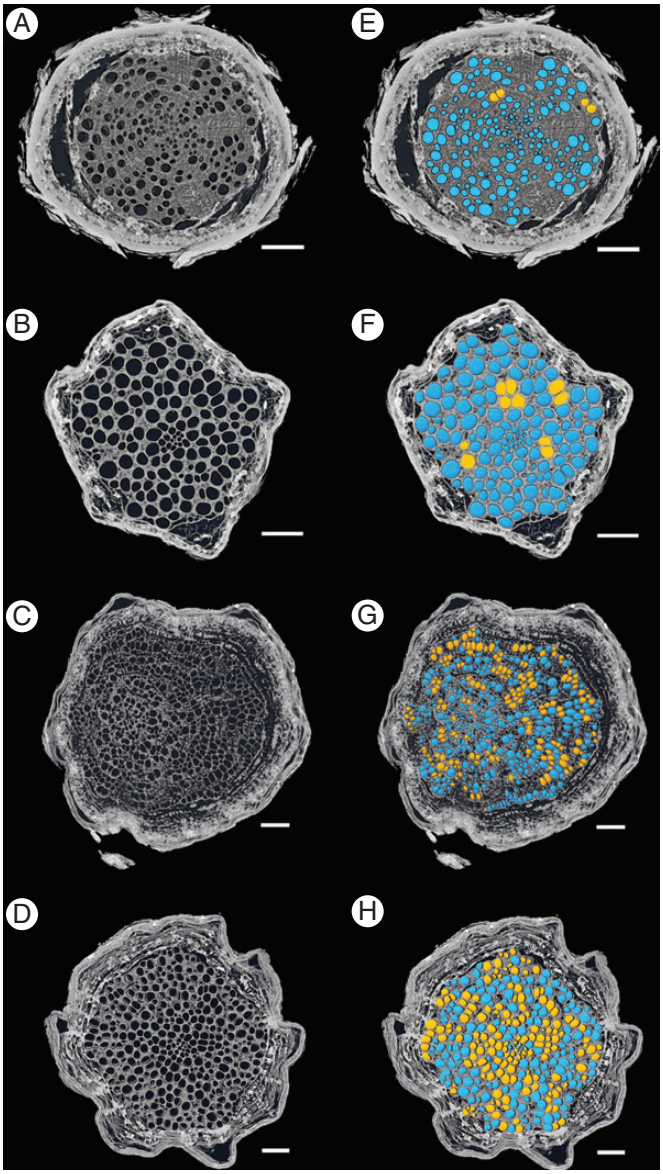

FIG. 1. Vessel connections in shallow roots of *Q. fusiformis* (A, E), deep roots of *Q. fusiformis* (B, F), shallow roots of *S. lanuginosum* (C, G) and deep roots of *S. lanuginosum* (D, H). Blue color indicates vessels with no observed connections, and yellow indicates vessels with at least one connection. Scale bars = 500 μm.

and shape of pits embedded in the vessel walls (Fig. 4). In both species, the pits were predominantly alternate, but occasionally scalariform or 'gash-like' (Fig. 4 C, H). Intervessel and vessel–tracheid alternate pitting was often interspersed with, or surrounded by, vessel–parenchyma scalariform pitting (Fig. 4). Deep *Q. fusiformis* roots had some extremely large pits (200–1000 μm^2 area) and this pit size class was not observed in either deep or shallow *S. lanuginosum* or shallow *Q. fusiformis* roots (Fig. 5). Pit area per vessel area was greater in shallow *S. lanuginosum* roots than in deep roots of the same species ($P < 0{\cdot}001$, Fig. 3B). However, in *Q. fusiformis*, pit area per vessel area was similar in deep and shallow roots. Transverse TEM imaging revealed that intervessel pit membranes were thicker in deep than in shallow roots of *Q. fusiformis* (Table 2;

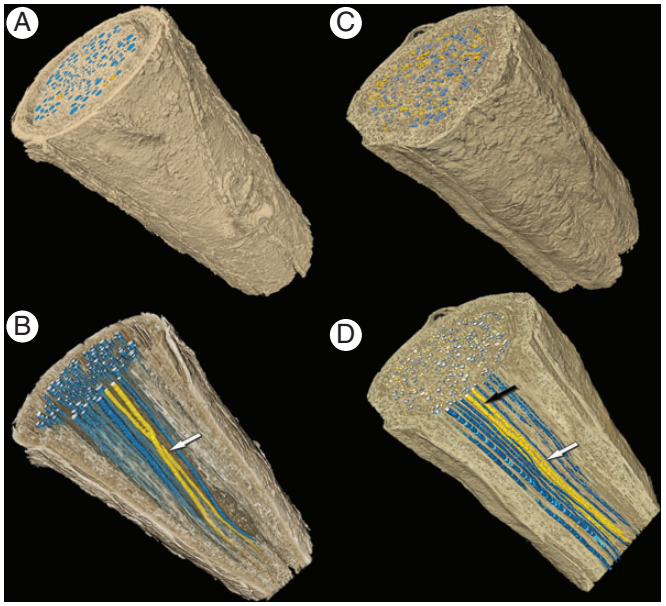

FIG. 2. Reconstruction of three-dimensional vessel networks and vessel connections in roots. A and B show a shallow *Q. fusiformis* root section and correspond to Fig. 1E. C and D show a shallow *S. lanuginosum* root section and correspond to Fig. 1G. Arrows indicate vessel–vessel connections.

$P = 0{\cdot}01$). However, membrane thickness was not significantly different in shallow vs. deep roots of *S. lanuginosum* ($P = 0{\cdot}11$).

Hydraulic capacity and cavitation resistance of the xylem networks

Based on average air-seeding pressures determined using the microcapillary technique, root vessels of *S. lanuginosum* were more vulnerable to embolism than those of *Q. fusiformis* (−0·6 vs. −2·2 MPa, respectively, $P < 0{\cdot}0001$, Fig. 3C), and deep root vessels were more vulnerable to embolism than vessels in shallow roots ($P = 0{\cdot}025$). There was no significant relationship between vessel air-seeding pressure and pit membrane thickness (Fig. 6A). However, there was a strong ($r^2 = 0{\cdot}82$, $P < 0{\cdot}0001$), positive relationship between vessel air-seeding pressure and the fraction of connected vessels (Fig. 6B). Based on our analysis of the vessel diameter distributions in each root sample, we calculated the theoretical root hydraulic conductivity (Table 3), which was greater in deep roots than in shallow roots due to the larger diameter vessels at that depth (Table 3). Surprisingly, we found no relationship between pit membrane thickness and calculated maximum pore diameter (based on air-seeding thresholds), but pore sizes were larger in shallow and deep *S. lanuginosum* [466·2 ± 144·52 nm (s.d.) and 889·9 ± 264·6 nm, respectively] compared with shallow and deep *Q. fusiformis* (134·9 ± 55·15 nm and 166·7 ± 50·54 nm, respectively), due to the differences in air-seeding thresholds.

DISCUSSION

There is little research on the microanatomy of woody plant roots, especially for vascular tissues (Carlquist, 1982; Machado *et al.*, 1997). Because the root xylem is of primary importance for water delivery to the plant, this lack of root studies is surprising.

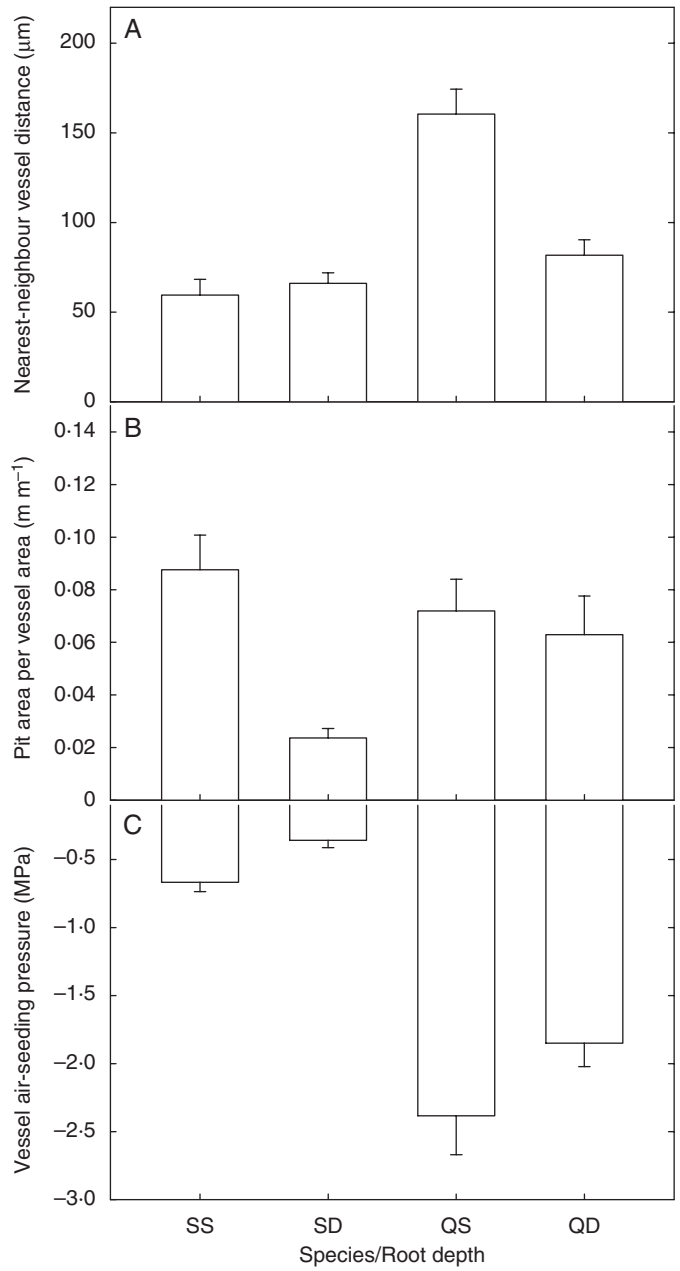

FIG. 3. Vessel pair distances, pit area per vessel area and individual vessel air-seeding pressures in deep and shallow roots of *Q. fusiformis* (QD and QS, respectively) and *S. lanuginosum* (SD and SS, respectively). (A) *Q. fusiformis* vessels are farther apart, particularly in shallow roots, than *S. lanuginosum* vessels. (B) Shallow roots of *S. lanuginosum* have more pit area per vessel area than deep roots of the same species. Pit area per vessel area is similar in deep and shallow *Q. fusiformis* roots. (C) *Q. fusiformis* root vessels are more resistant to embolism than *S. lanuginosum* root vessels, and shallow root vessels are more resistant than deep root vessels. Error bars are the standard errors.

The relative ease of studying above-ground plant tissue compared with the root system is largely responsible for this disparity, but access to the deep cave roots allows us to measure root anatomical and physiological parameters on samples that would otherwise be unobtainable.

In this study, we compared the root xylem anatomy in two co-occurring species with different vessel arrangements: one with a hydraulically modular system (*Q. fusiformis*) and one with a hydraulically integrated system (*S. lanuginosum*). Despite having only a moderate number of individuals and measurements, several important relationships emerged from this study. Pit size and shape varied markedly and was most probably related to the cell type to which it was connected (i.e. tracheid, vessel or parenchyma) (Wheeler, 2011). The largest pits, which were scalariform in shape in both *Q. fusiformis* and *S. lanuginosum*, were most probably vessel–parenchyma pits (Wheeler and Thomas, 1981; Carlquist, 2001). The presence of these large vessel–parenchyma pits suggests that there is likely to be considerable water movement between vessels and parenchyma in both species. It should be noted that roots of many angiosperm species are highly vulnerable to embolism (McElrone *et al.*, 2004; Maherali *et al.*, 2006) and xylem parenchyma is the most likely source for embolism repair (Brodersen *et al.*, 2010; Secchi and Zwieniecki, 2011; Johnson *et al.*, 2012).

TABLE 1. *Vessel density (number of vessels per mm^2) and vessel connections in deep and shallow roots of* S. lanuginosum *and* Q. fusiformis *assessed using HRCT images (mean ± s.d.)*

Species/depth	Vessel density	No. of vessel connections	Total no. of vessels observed	Fraction of vessels with connections
S. lanuginosum shallow	14·7 ± 9·3	409	1211	0·34
S. lanuginosum deep	20·9 ± 5·0	576	1295	0·44
Q. fusiformis shallow	11·4 ± 4·3	4	548	0·01
Q. fusiformis deep	16·9 ± 6·7	14	224	0·06

In the current study, *Q. fusiformis* root vessels were resistant to embolism via air seeding, but vessels of *S. lanuginosum* were highly vulnerable. This is in contrast to earlier work showing that both *Q. fusiformis* and *S. lanuginosum* roots were highly vulnerable to embolism (loss of 50 % conductivity at pressures $<$0·8 MPa; McElrone *et al.*, 2004). There has been much discussion in the literature concerning appropriate methods for measuring hydraulic vulnerability in species with long vessels, including oaks in particular (Li *et al.*, 2008; Choat *et al.*, 2010; Cochard *et al.*, 2010, 2013; Ennajeh *et al.*, 2011; Wheeler *et al.*, 2013), and recent work suggests that hydraulic vulnerability measurements on segments longer than the longest vessel are reliable (e.g. Christman *et al.*, 2012). However, the choice of method (e.g. centrifuge, air injection or benchtop dehydration) should be carefully considered and appropriately matched to the species being studied (Choat *et al.*, 2010; McElrone *et al.*, 2012). It is likely that in McElrone *et al.* (2004), several early-wood vessels embolized at very low pressures or that the samples used were not longer than the longest vessel. Either of these scenarios would result in large losses in overall root hydraulic conductance at very low pressures. There were probably highly vulnerable vessels in the *Q. fusiformis* roots that were used in the current study, but they were not sampled. Here, we generated air-seeding measurements by testing the integrity of individual vessels rather than the entire network as a whole. Vessel networks can be thought of as populations of individual vessels having differing degrees of embolism resistance. For

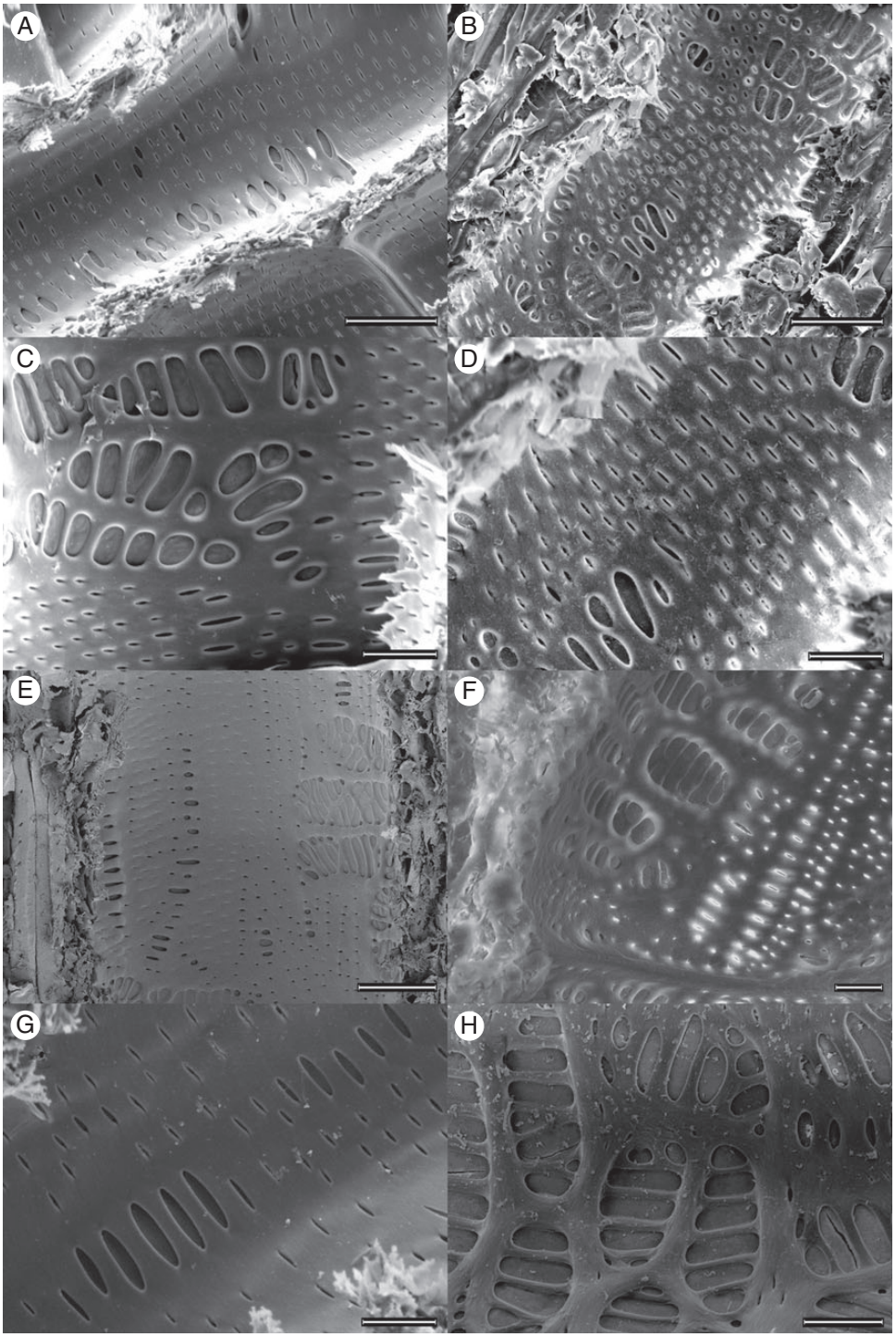

FIG. 4. Environmental scanning electron microscopy images of *Sideroxylon lanuginosum* (A, C, E, G) and *Quercus fusiformis* (B, D, F, H) shallow (A–D) and deep (E–H) roots showing the large degree of variability in pit shape and size. Scale bars are (A, B) 50 μm, (C, D) 20 μm, (E) 50 μm and (F–H) 20 μm.

example, in stems of *Quercus gambelii*, individual vessel air-seeding pressures ranged from 0·1 to >5 MPa (Christman *et al.*, 2012). This phenomenon is probably due to the relationships between intervessel connectivity (i.e. total pit area), pit membrane thickness and porosity.

Vessels in *Q. fusiformis* were on average further apart than those in *S. lanuginosum*, and *Q. fusiformis* had fewer vessel connections than in *S. lanuginosum*. Only 1–6 % of vessels were connected in *Q. fusiformis*, but 34–44 % were connected in *S. lanuginosum*. Previous work has shown that greater hydraulic integration is related to more vulnerable xylem (Loepfe *et al.*, 2007; Brodersen *et al.*, 2012) and is more common in mesic habitats (Schenk *et al.*, 2008). In contrast, earlier work by Carlquist (1966, 1984) showed that the degree of vessel

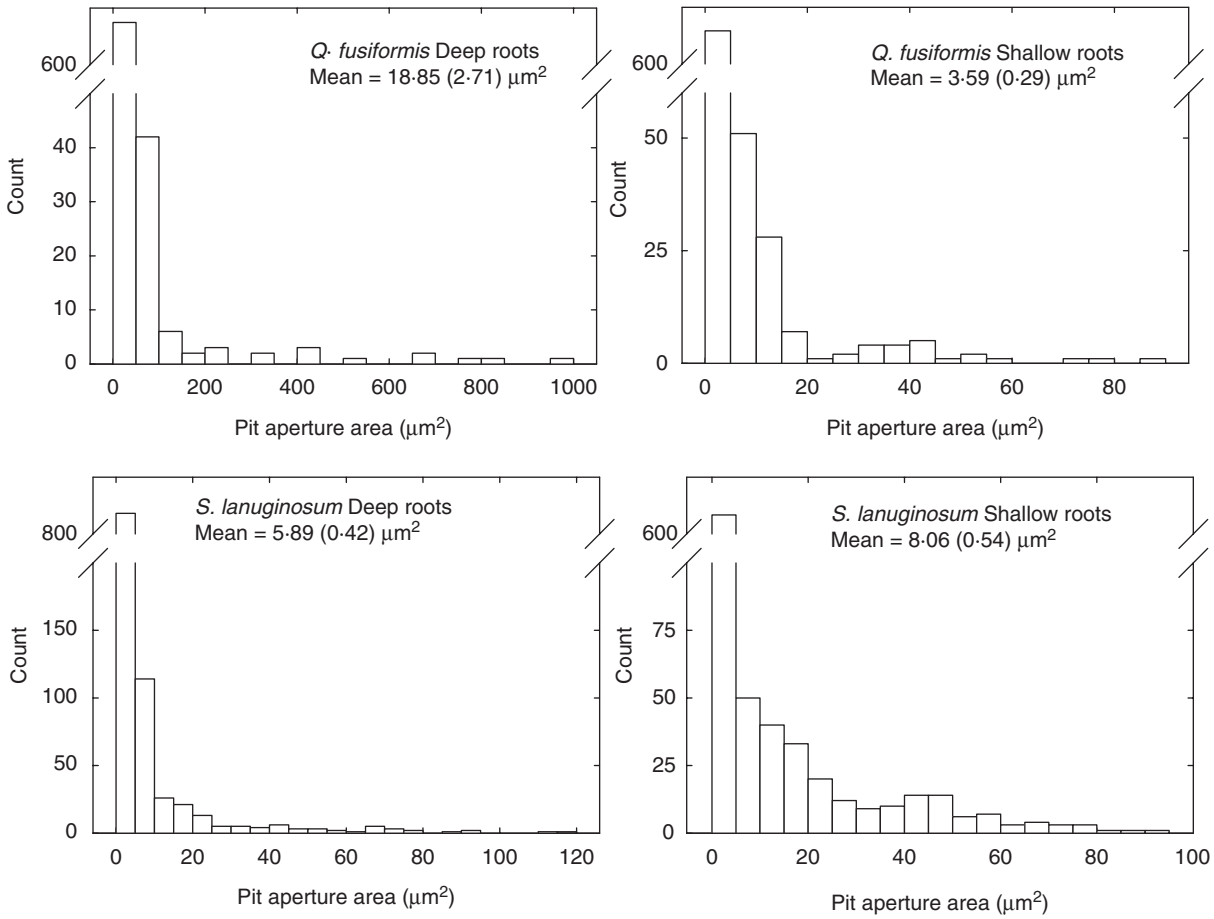

FIG. 5. Root pit area histograms. Note the large difference in the scale of the *x*-axes. Deep roots of *Q. fusiformis* have many more large pits than other samples and also have the largest individual pits (>500 μm²). Numbers in parentheses are the standard errors.

TABLE 2. *Pit membrane thickness and estimated pore diameter in deep and shallow roots of* S. lanuginosum *and* Q. fusiformis *(mean ± s.e.)*

Species/depth	Pit membrane thickness (μm)	Pit membrane pore diameter (μm)
S. lanuginosum shallow	0·333 ± 0·03	0·466 ± 0·07
S. lanuginosum deep	0·308 ± 0·03	0·890 ± 0·12
Q. fusiformis shallow	0·239 ± 0·03	0·134 ± 0·02
Q. fusiformis deep	0·410 ± 0·04	0·167 ± 0·02

interconnectedness was positively correlated with aridity. However, the two species in the current study have vasicentric tracheids (i.e. tracheids surrounding vessels; Metcalfe and Chalk, 1950; Carlquist, 1984), and species with vasicentric tracheids appear to be an exception to this general trend. Also, hydraulic integration can result in greater ion-mediated increases in hydraulic conductivity (Jansen *et al.*, 2011). This observation could be particularly important in species growing in karst (as our species were), as there is probably a high concentration of dissolved limestone in underground streams.

Recently, Brodersen *et al.* (2013) showed that xylem organization plays a critical role in the spread of drought-induced embolism in grapevine. In young stems, embolisms spread radially from the stem centre toward the epidermis, moving though intervessel connections. Because of the sectored nature of grapevine xylem, embolism spread was largely confined to individual vessel groups, and the lack of lateral connections between vessels prevented systemic spread. Here, deep *Q. fusiformis* roots observed in cross-section appeared to be more highly integrated than shallow roots (Fig. 1). Indeed, deep *Q. fusiformis* root vessels were more highly connected than those in shallow roots (6 % vs. 1 %, respectively). However, because root vessel length is known to be long in general (e.g. Zimmermann and Potter 1982), our connectivity data based on short samples potentially underestimate the connectivity in each sample group. However, it is worth noting the strong relationship between air-seeding pressures, which were determined on 6 cm long segments, and the degree of vessel connectivity, measured on 7 mm long segments (Fig. 6). This suggests that even using short samples, a good estimate of vessel connectivity may be obtained using these methods.

The greater resistance to air seeding and the more sectored organization visible in the shallow *Q. fusiformis* roots (Fig. 1, Table 1) support the idea that cavitation resistance increases

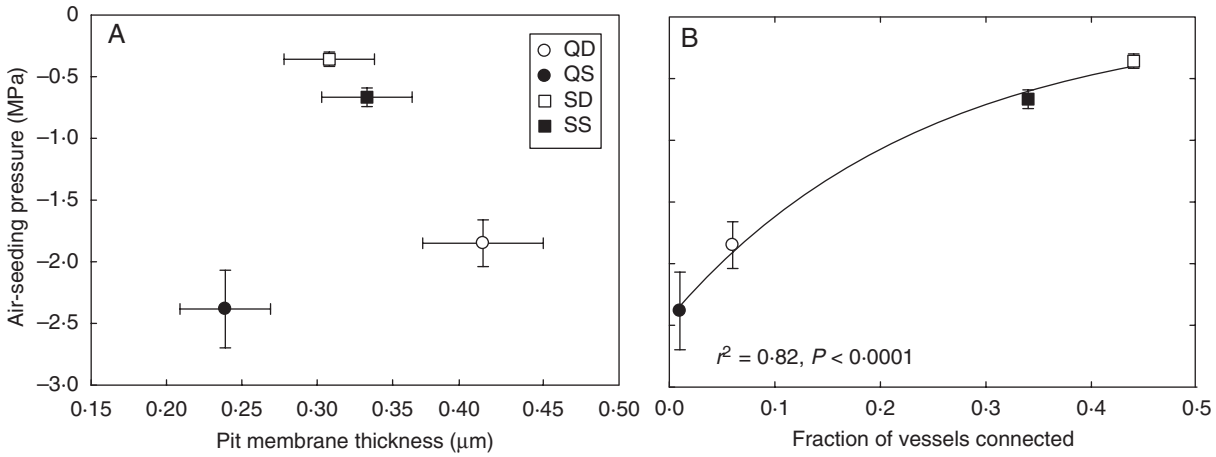

FIG. 6. Air-seeding pressure is not related to pit membrane thickness (A) but shows a strong relationship with the fraction of vessels connected (B). Error bars are the standard errors.

TABLE 3. *Theoretical vs. measured root conductivity*

Species/depth	Measured K_s	Theoretical K_s	Percentage difference (%)
S. lanuginosum shallow	9·5	24·9	−61·8
S. lanuginosum deep	22	121·2	−81·8
Q. fusiformis shallow	14	46·4	−70·0
Q. fusiformis deep	43	197·4	−78·2

Measured data are from McElrone *et al.* (2004).

Specific conductivity (K_s) values are in kg m^{-1} s^{-1} MPa^{-1}. Vessel diameters used to calculate theoretical conductivity are presented in Supplementary Data Fig. S1.

with increased distance from the water source. With deep *Q. fusiformis* roots being more vulnerable to air seeding, we expected pit membranes to be thinner in deep vessels compared with shallow vessels. However, we found the opposite in *Q. fusiformis* and found no significant difference in pit membrane thickness between deep and shallow roots of *S. lanuginosum* (Table 2). Therefore, these data suggest that xylem network connectivity is a critical component of cavitation resistance in these two species.

Pit membrane thickness is often related to vessel air-seeding pressure, with thicker pit membranes being more resistant to air seeding (Choat *et al.*, 2003; Lens *et al.*, 2011). Pit membrane pore sizes have also been correlated with vessel air-seeding pressures, and species with thicker pit membranes often have smaller diameter pores in the pit membrane (Jansen *et al.*, 2009). In our study, vessel air-seeding pressure was not related to pit membrane thickness, and both *Q. fusiformis* and *S. lanuginosum* had no visible pores in pit membranes at a magnification of ×25 000 (D. M. Johnson, unpubl. data). Additionally, Jansen *et al.* (2009) found no visible pores in pit membranes of *Quercus robur* at a similar magnification. Following the methods of Jansen *et al.* (2009), we calculated the theoretical maximum pore diameter within the pit membrane based on the air-seeding data generated using the microcapillary technique, and found no relationship between pore size and pit membrane thickness. Calculated pore diameters from both species and depths ranged from 88·1 to 1163·5 nm and, given that a single large diameter pore is the only requirement for embolisms to spread (the 'rare pit' hypothesis, Christmann *et al.*, 2009, 2012), the infrequency of large pores probably meant that they eluded our efforts to detect them using SEM.

The percentage difference in theoretical vs. measured conductivity was greater in deep roots than in shallow roots. This result suggests that pit membranes account for a larger portion of the overall xylem hydraulic resistance in deep roots than in shallow roots. Although there are large differences in vessel–vessel connections between the two species, there are not large discrepancies between the theoretical and measured percentage differences in hydraulic conductivity. This is surprising given that the reasons for the difference in the theoretical vs. measured conductivities are end wall effects and pit hydraulic resistances (Hacke *et al.*, 2006; Choat *et al.*, 2008). Because of the high frequency of vessel–vessel connections in *S. lanuginosum*, one would expect that multiple pit–pair crossings would contribute a substantial portion of the overall hydraulic resistance of the vessel network. One unexplored facet of the hydraulic network in these species is the presence of vasicentric tracheids. Although these tracheids are, on average, only 2–3 % as wide as the vessels that they surround (data from the InsideWood Database, http://insidewood.lib.ncsu.edu; Wheeler, 2011), they are connected to the adjacent vessels. Carlquist (1984) has proposed that these tracheids provide a 'back-up' hydraulic transport system when the vessels embolize. Based on Hagen–Poiseuille calculations, the vessels should be of the order of 10^6 more conductive than the adjacent tracheids, but the tracheids could provide at least some degree of flow during extreme drought, or they may contribute capacitive water to the transpiration stream.

Our current study highlights the need for future research on root microanatomy and hydraulic functioning. Advancements in this research area should include studies that examine the relationship between vessel vulnerability to embolism and hydraulic integration across a wide variety of species and habitats. Utilizing the new developments in non-destructive 3-D imaging demonstrated in this study will allow researchers to measure longer stem and root segments to better understand the complexity of

vessel network integration throughout the plant. Previous studies have identified vessel diameter, pit membrane thickness and pit pore diameter as network properties that influence vessel vulnerability to embolism (Jansen *et al.*, 2009; Lens *et al.*, 2011). By generating 3-D reconstructions of the xylem network, and incorporating those key network properties, researchers can use mathematical simulations to estimate which network components contribute the most to hydraulic conductivity and cavitation resistance (e.g. Loepfe *et al.* 2007; Lee *et al.*, 2013). Recent research has shown that modelling the connections between vessels using HRCT imaging can reveal emergent properties of the xylem network that would otherwise be difficult to study (Lee *et al.*, 2013). Future research integrating these traits with 3-D xylem connectivity may result in a better understanding of the fundamental relationships between xylem structure and function.

SUPPLEMENTARY DATA

Supplementary data are available online at www.aob.oxfordjournals.org and consist of Figure S1: frequency histograms of vessel diameters in deep and shallow roots of *Q. fusiformis* and *S. lanuginosum*.

ACKNOWLEDGEMENTS

This work was funded by NSF IOS-0920355 and a grant from USDA-AFRI. We thank Phillip Fay, Anne Gibson and Kyle Tiner for assistance in co-ordination of field campaigns, and A. MacDowell and D. Parkinson for their assistance at the Lawrence Berkeley National Laboratory Advanced Light Source Beamline 8·3.2 in Berkeley, CA, USA, where the HRCT imaging was performed. The Advanced Light Source is supported by the Director, Office of Science, Office of Basic Energy Services, of the US Department of Energy under contract no. DE-AC01-05CH11231.

LITERATURE CITED

Bleby TM, McElrone AJ, Jackson RB. 2010. Water uptake and hydraulic redistribution across large woody root systems to 20 m depth. *Plant, Cell and Environment* **33**: 2132–2148.

Brodersen CR, McElrone AJ, Choat B, Matthews MA, Shackel KA. 2010. Dynamics of embolism repair in grapevine: *in vivo* visualizations using HRCT. *Plant Physiology* **154**: 1088–1095.

Brodersen CR, Lee E, McElrone AJ, Choat B, Shackel KA, Phillips R, Matthews MA. 2011. Automated analysis of three-dimensional xylem networks using high-resolution computed tomography. *New Phytologist* **191**: 1168–1179.

Brodersen CR, Roark LC, Pitterman J. 2012. The physiological implications of primary xylem organization in two ferns. *Plant, Cell and Environment* **35**: 1898–1911.

Brodersen CR, Lee E, Choat B, Shackel K, McElrone A, Matthews A. 2013. *In vivo* visualizations of drought-induced embolism spread in *Vitis vinifera*. *Plant Physiology* **161**: 1820–1829.

Canadell J, Jackson RB, Ehleringe JR, Mooney HA, Sala OE, Schulze E-D. 1996. Maximum rooting depth of vegetation types at the global scale. *Oecologia* **108**: 583–595.

Carlquist S. 1966. Wood anatomy of Compositae: a summary, with comments on factors controlling wood evolution. *Aliso* **6**: 25–44.

Carlquist S. 1982. Wood anatomy of Onagraceae: further species; root anatomy; significance of vestured pits and allied structures in dicotyledons. *Annals of the Missouri Botanical Garden* **69**: 755–769.

Carlquist S. 1984. Vessel grouping in dicotyledon wood: significance and relationship to imperforate tracheary elements. *Aliso* **10**: 505–525.

Carlquist S. 2001. *Comparative wood anatomy*. Berlin: Springer.

Choat B, Ball M, Luly J, Holtum J. 2003. Pit membrane porosity and water stress-induced cavitation in four co-existing dry rainforest tree species. *Plant Physiology* **131**: 41–48.

Choat B, Lahr EC, Melcher PJ, Zwieniecki MA, Holbrook NM. 2005. The spatial pattern of air seeding thresholds in mature sugar maple trees. *Plant, Cell and Environment* **28**: 1082–1089.

Choat B, Brodie TW, Cobb AR, Zwieniecki MA, Holbrook NM. 2006. Direct measurements of intervessel pit membrane hydraulic resistance in two angiosperm tree species. *American Journal of Botany* **93**: 993–1000.

Choat B, Cobb AR, Jansen S. 2008. Structure and function of bordered pits: new discoveries and impacts on whole-plant hydraulic function. *New Phytologist* **177**: 608–626.

Choat B, Drayton WM, Brodersen C, Matthews MA, Schackel KA, Wada H, McElrone AJ. 2010. Measurement of vulnerability to water stress-induced cavitation in grapevine: a comparison of four techniques applied to a long vesseled species. *Plant, Cell and Environment* **33**: 1502–1512.

Christman MA, Sperry JS, Adler FR. 2009. Testing the 'rare pit' hypothesis in three species of *Acer*. *New Phytologist* **182**: 664–674.

Christman MA, Sperry JS, Smith DD. 2012. Rare pits, large vessels, and extreme vulnerability to cavitation in a ring-porous tree species. *New Phytologist* **193**: 713–720.

Cochard H, Herbette S, Barigah T, Vilagrosa A. 2010. Does sample length influence the shape of vulnerability to cavitation curves? A test with the Cavitron spinning technique *Plant, Cell and Environment* **33**: 1543–1552.

Cochard H, Badel E, Herbette S, Delzon S, Choat B, Jansen S. 2013. Methods for measuring plant vulnerability to cavitation: a critical review. *Journal of Experimental Botany* **64**: 4779–4791.

Cruiziat P, Cochard H, Ameglio T. 2002. Hydraulic architecture of trees: main concepts and results. *Annals of Forest Science* **7**: 723–752.

David TS, David JS, Pinto CA, Cermak J, Nadezhdin V, Nadezhdina N. 2012. Hydraulic connectivity from roots to branches depicted through sap flow: analysis on a *Quercus suber* tree. *Functional Plant Biology* **39**: 103–115.

Domec J-C, Scholz FG, Bucci SJ, Meinzer FC, Goldstein G, Villalobos Vega R. 2006. Diurnal and seasonal variation in root xylem embolism in neotropical savanna woody species: impact on stomatal control of plant water status. *Plant, Cell and Environment* **29**: 26–35.

Ennajeh M, Simoes F, Khemira H, Cochard H. 2011. How reliable is the double-ended pressure sleeve technique for assessing xylem vulnerability to cavitation in woody angiosperms? *Physiologia Plantarum* **142**: 205–210.

Hacke UG, Sperry JS, Wheeler JK, Castro L. 2006. Scaling of angiosperm xylem structure with safety and efficiency. *Tree Physiology* **26**: 619–701.

Hargrave KR, Kolb KJ, Ewers FW, Davis SD. 1994. Conduit diameter and drought-induced embolism in *Salvia mellifera* Greene (Labiatae). *New Phytologist* **126**: 695–705.

Jackson RB, Moore LA, Hoffmann WH, Pockman WT, Linder CR. 1999. Ecosystem rooting depth determined with caves and DNA. *Proceedings of the National Academy of Sciences, USA* **96**: 11387–11392.

Jackson RB, Sperry JS, Dawson TE. 2000. Root water uptake and transport: using physiological processes in global predictions. *Trends in Plant Science* **5**: 482–488

Jacobsen AL, Pratt RB, Davis SD, Ewers FW. 2007. Cavitation resistance and seasonal hydraulics differ among three arid Californian plant communities. *Plant, Cell and Environment* **30**: 1599–1609.

Jansen S, Choat B, Pletsers A. 2009. Morphological variation of intervessel pit membranes and implications to xylem function in angiosperms. *American Journal of Botany* **96**: 409–419.

Jansen S, Gortan E, Lens F, Lo Gullo MA, Salleo S, Scholz A. 2011. Do quantitative vessel and pit characters account for ion-mediated changes in the hydraulic conductance of angiosperm xylem? *NewPhytologist* **189**: 218–228.

Johnson DM, McCulloh KA, Woodruff DR, Meinzer FC. 2012. Hydraulic safety margins and embolism reversal in stems and leaves: why are conifers and angiosperms so different? *Plant Science* **195**: 48–53.

Johnson DM, Domec- J-C, Woodruff DR, McCulloh KA, Meinzer FC. 2013. Contrasting hydraulic strategies in two tropical lianas and their host trees. *American Journal of Botany* **100**: 374–383.

Lee EF, Matthews MA, McElrone AJ, Phillips RJ, Shackel KA, Brodersen CB. 2013. Analysis of HRCT-derived xylem network reveals reverse flow in some vessels. *Journal of Theoretical Biology* **333**: 146–155.

Lens F, Sperry JS, Christman MA, Choat B, Rabaey D, Jansen S. 2011. Testing hypotheses that link wood anatomy to cavitation resistance and hydraulic conductivity in the genus *Acer*. *New Phytologist* **190**: 709–723.

Li Y, Sperry JS, Taneda H, Bush SE, Hacke UG. 2008. Evaluation of centrifugal methods for measuring xylem cavitation in conifers, diffuse- and ring-porous angiosperms. *New Phytologist* **177**: 558–568.

Loepfe L, Martinez-Vilalta J, Piñol J, Mencuccini M. 2007. The relevance of xylem network structure for plant hydraulic efficiency and safety. *Journal of Theoretical Biology* **247**: 788–803.

Luu D-T, Maurel C. 2005. Aquaporins in a challenging environment: molecular gears for adjusting plant water status. *Plant, Cell and Environment* **28**: 85–96.

Machado SR, Angyalossy-Alfonso V, De Morretes BL. 1997. Comparative wood anatomy of root and stem in *Styrax camporum* (Styracaceae). *IAWA Journal* **18**: 13–25.

Maherali H, Moura CF, Caldeira MC, Willson CJ, Jackson RB. 2006. Functional coordination between leaf gas exchange and vulnerability to xylem cavitation in temperate forest trees. *Plant, Cell and Environment* **29**: 571–583.

Maurel C, Verdoucq L, Luu D-T, Santoni V. 2008. Plant aquaporins: membrane channels with multiple integrated functions *Annual Review of Plant Biology* **59**: 595–624.

McElrone AJ, Pockman WT, Martinez-Vilalta J, Jackson RB. 2004. Variation in xylem structure and function in stems and roots of trees to 20 m depth. *New Phytologist* **163**: 507–517.

McElrone AJ, Bichler J, Pockman WT, Addington RN, Linder CR, Jackson RB. 2007. Aquaporin-mediated changes in hydraulic conductivity of deep tree roots accessed via caves. *Plant, Cell and Environment* **30**: 1411–1421.

McElrone AJ, Brodersen C, Alsina MM, *et al*. 2012. Centrifuge technique consistently overestimates vulnerability to water-stress induced cavitation in grapevines as confirmed with high resolution computed tomography. *New Phytologist* **196**: 661–665.

Metcalfe CR, Chalk L. 1950. *Anatomy of the dicotyledons.* Oxford: Clarendon Press.

Oliviera RS, Bezerra L, Davidson EA, Pinto F, Klink CA, Nepstad DC, Moreira A. 2005. Deep root function in soil water dynamics in cerrado savannas of central Brazil. *Functional Ecology* **19**: 574–581.

Orians CM, Babst BB, Zanne AE. 2005. Vascular constraints and long distance transport in dicots. In: Holbrook NM, Zwieniecki MA, eds. *Vascular transport in plants*. Amsterdam: Elsevier, 355–371.

Pratt RB, Jacobsen AL, Ewers FW, Davis SD. 2007. Relationships among xylem transport, biomechanics and storage in stems and roots of nine Rhamnaceae species of the California chaparral. *New Phytologist* **174**: 787–798.

Secchi F, Zwieniecki MA. 2011. Sensing embolism in xylem vessels: the role of sucrose as a trigger for refilling. *Plant, Cell and Environment* **34**: 514–524.

Schenk HJ, Jackson RB. 2002. Rooting depths, lateral spreads, and belowground/aboveground allometries of plants in water limited ecosystems. *Journal of Ecology* **90**: 480–494.

Schenk HJ, Jackson RB. 2005. Mapping the global distribution of deep roots in relation to climate and soil characteristics. *Geoderma* **126**: 129–140.

Schenk HJ, Espino S, Goedhart CM, Nordenstahl M, Martinez-Cabrera HI, Jones CS. 2008. Hydraulic integration and shrub growth form linked across continental aridity gradients. *Proceedings of the National Academy of Sciences, USA* **105**: 11248–11253.

Sperry JS, Pockman WP. 1993. Limitation of transpiration by hydraulic conductance and xylem cavitation in *Betula occidentalis*. *Plant, Cell and Environment* **16**: 279–288.

Steudle E, Petersen CA. 1998. How does water get through roots? *Journal of Experimental Botany* **49**: 775–788.

Tyree MT, Ewers FW. 1991. Tansley Review 34. The hydraulic architecture of trees and other woody plants. *New Phytologist* **119**: 345–360.

Tyree MT, Zimmermann MH. 2002. *Xylem structure and the ascent of sap*. Berlin: Springer.

Waisel Y, Liphschitz N, Kuller Z. 1972. Patterns of water movement in trees and shrubs. *Ecology* **53**: 520–523.

West AG, Hultine KR, Jackson TL, Ehleringer JR. 2007. Differential summer water use by *Pinus edulis* and *Juniperus osteosperma* reflects contrasting hydraulic characteristics. *Tree Physiology* **27**: 1711–1720.

Wheeler EA. 2011. InsideWood – a web resource for hardwood anatomy. *IAWA Journal* **32**: 199–211.

Wheeler EA, Thomas RJ. 1981. Ultrastructural characteristics of mature wood of southern red oak (*Quercus falcata* Michx.) and white oak (*Quercus alba* L.). *Wood and Fiber* **13**: 169–181.

Wheeler JK, Huggett BA, Tofte AN, Rockwell FE, Holbrook NM. 2013. Cutting xylem under tension or supersaturated with gas can generate PLC and the appearance of rapid recovery from embolism. *Plant, Cell and Environment* **36**: 1938–1949.

Wiebe HH, Brown RW. 1970. Water potential measurements in trees. *BioScience* **20**: 225–226.

Zimmermann MH, Brown CL. 1971. *Trees: structure and function*. New York: Springer-Verlag.

Zimmermann MH, Potter D. 1982. Vessel-length distribution in branches, stem and roots of *Acer rubrum* L. *IAWA Bulletin* **3**: 103–109.

Zwieniecki MA, Holbrook NM. 1998. Diurnal variation in xylem hydraulic conductivity in white ash (*Fraxinus americana* L.), red maple (*Acer rubrum* L.) and red spruce (*Picea rubens Sarg.*). *Plant, Cell and Environment* **21**: 1173–1180.